# Lateral Inverse Proximity Effect in Ti/Au Transition Edge Sensors

Nagayoshi, K.; de Wit, M.; Taralli, E.; Visser, S.; Ridder, M. L.; Gottardi, L.; Akamatsu, H.; Vaccaro, D.; Gao, J. R.; More Authors

**DOI**
10.1007/s10909-022-02828-3

**Publication date**
2022

**Document Version**
Final published version

**Published in**
Journal of Low Temperature Physics

Journal of Low Temperature Physics
https://doi.org/10.1007/s10909-022-02828-3

# Lateral Inverse Proximity Effect in Ti/Au Transition Edge Sensors

**K. Nagayoshi[1] · M. de Wit[1] · E. Taralli[1] · S. Visser[1] · M. L. Ridder[1] · L. Gottardi[1] · H. Akamatsu[1] · D. Vaccaro[1] · M. P. Bruijn[1] · J.-R. Gao[1,2] · J. W. A. den Herder[1,3]**

Received: 2 November 2021 / Accepted: 1 August 2022


**Abstract**
We report measured $T_c$ of superconducting Ti/Au bilayer strips with a width $W$ varying from 5 to 50 μm. The strips were fabricated based on a Ti/Au bilayer that consists of a 41-nm-thick Ti layer to which a 280-nm-thick Au layer was added. We find that the $T_c$ drops as $W$ decreases and the declining trend almost perfectly follows $T_c/[\mathrm{mK}] = -738.4[\mu\mathrm{m}]^2/W^2 + 91.0$, where $T_c(W = \infty)$ of 91 mK is consistent with the intrinsic $T_c$ of the bilayer. The result is interpreted as a consequence of the lateral inverse proximity effect originated in normal-metal microstructures, namely Au overhangs that exist at the edges of the Ti/Au bilayer. The $T_c$ shift from the intrinsic $T_c$ should be anticipated in addition to the longitudinal proximity effect from superconducting Nb leads when one designs Ti/Au TESs.

**Keywords** Ti/Au · Bilayer · TES · Proximity effect · X-ray · Microcalorimeter · Athena · X-IFU

## 1 Introduction

Superconducting transition-edge sensors (TESs) [1] can achieve very high sensitivities at low temperature in almost any wavelength bands. There are many aspects to be considered thoughtfully when designing TESs for space/ground-based applications. However, superconducting transition temperature $T_c$ is one of the most

✉ K. Nagayoshi
K.Nagayoshi@sron.nl

1 NWO-I/SRON Netherlands Institute for Space Research, Niels Bohrweg 4, 2333 CA Leiden, The Netherlands

2 Faculty of Applied Science, Delft University of Technology, Lorentzweg, 2628 CJ Delft, The Netherlands

3 Astronomical Institute Anton Pannekoek, University of Amsterdam, Science Park 904, 1098XH Amsterdam, The Netherlands

Published online: 16 August 2022

important parameters to be tuned precisely because it is essentially associated with a detector sensitivity and a signal bandwidth. In many cases, TESs are fabricated with proximity-coupled normal-metal/superconductor bilayers because $T_c$ can be adjusted relatively straightforward in a wide target range. $T_{ci}$, defined as an intrinsic $T_c$ to be observed for an infinitely wide bilayer, is roughly speaking determined by the thickness of each layer and interface transmissivity. However, $T_c$ of real TES devices are known to be different from $T_{ci}$. This $\Delta T_c = T_c - T_{ci}$ is thought to be originated in two additional in-plane proximity effects: the longitudinal proximity effect and the lateral inverse proximity effect. These effects were firstly reported by Sadleir et al. [2, 3] on devices based on square Mo/Au TESs of different sizes with or without additional normal-metal structure such as "banks" and interdigitated "fingers" made of Au. The main points are briefly summarized as follows:

- $\Delta T_c$ and the transition width of a superconducting RT (resistance vs. temperature) curve are scaled with $1/L^2$, where $L$ is a spacing between superconducting leads directly attached on a TES. This is interpreted that superconductivity is enhanced by the leads longitudinally in the bilayer.
- $\Delta T_c$ is scaled with $-1/s^2$, where $s$ is a spacing between the normal-metal structures. In this case superconductivity is suppressed laterally in the bilayer. The banks at the edges of a TES do not seem to have much to do with the transition width.

We are developing TES microcalorimeters based on a bare Ti/Au bilayer in the framework of a European sensor backup for the Athena/X-IFU instrument [4]. We have reported in de Wit et al. [5] that an excellent spectral performance of below 2 eV at 5.9 keV was achieved under AC-bias with high-aspect-ratio TESs, of which widths $W$ were designed to be much shorter than the lengths. In the same paper, we shortly mentioned that $\Delta T_c$ observed for the TESs with $W = 20$, 30, 40 μm follows a scaling law $-1/W^2$. We suggested that Au "overhangs" that exist at the edges of the Ti/Au bilayer (described in detail in Sect. 2) could suppress superconductivity in the bilayer as well as normal-metal banks do. However at that time, our understanding regarding this unique microstructure was limited and obviously more $T_c$ measurement data in the range of $W < 20$ μm was needed to characterize the scaling formula precisely.

In this paper, we examined the Au overhang microstructure in details. We report $T_c$ observed for superconducting Ti/Au strips with $W$ ranging from 5 to 50 μm, revealing the lateral inverse proximity effect on our Ti/Au bilayer.

## 2 Design and Fabrication of Test Samples

In Fig. 1a, we show a schematic of a test sample of which $T_c$ was characterized in this paper. It consists of a Ti/Au bilayer patterned into a strip shape lithographically and Nb/Ta superconducting leads directly deposited on the strip with a lift-off process. We designed the strips with the widths of 5.5, 8, 10, 15, 20, 30 and 50 μm that are fitted within a 11 mm square Si chip. The lengths of the strips were set to 5000

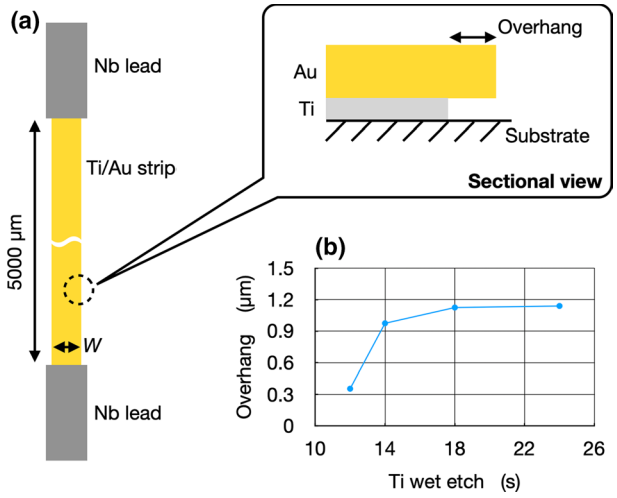


**Fig. 1** **a** Schematic of a Ti/Au strip. The Inset schematic shows a cutting view of a microstructure at the edge of the bilayer. The Au overhang is formed due to an undercut while etching the Ti layer. **b** Growth rate of the Au overhang measured with sacrificial samples of which Ti layers were etched for 12, 14, 18 and 24 s. Subsequent to the Ti etch, the Au layer for each sample was completely removed and the width of the Ti layer was directly inspected to determine the overhang distance (color figure online)

µm so that the longitudinal proximity effect has very little impact on $T_c$ and the transition width [6]. In this way, we can easily and accurately determine $T_c$ for each strip with a sharp RT curve, securing the robustness of our experiment. The Ti/Au bilayer consists of a 41-nm-thick Ti layer to which a 280-nm-thick Au layer was added anticipating the intrinsic $T_c$ of about 90 mK. More details about the deposition process of the Ti/Au bilayer can be found in [7]. The Ti/Au bilayer was patterned with wet processes at room temperature. The Au layer was etched with an iodine/iodide solution (prepared with a mixing ratio of KI : $I_2$ : $H_2O$ = 20 g : 5 g : 300 ml) for 55 s, followed by etching of the Ti layer with a dilute hydrofluoric acid solution (1%).

Here, the etching time of the Ti layer is crucial because the Au overhang indicated in the inset of Fig. 1a is formed by an undercut while etching the Ti layer. Figure 2 shows a typical Au overhang structure observed by using a SEM combined with a focused-ion-beam instrument. We beforehand investigated the growth rate of the Au overhang as presented in Fig. 1b. With an extrapolation from the data, the Au overhang starts being created about 11.5 s and rapidly grows to ~ 1 µm in the next few seconds, and then gradually saturates around 1.2 µm over the next 10 s. As a preliminarily test, we evaluated $T_c$ of two 50-µm-wide Ti/Au strips prepared with different Au overhang widths. These samples were fabricated on a Si wafer coated with SiN and measured following the same manner described in details in Sect. 3. As shown in Fig. 3, $T_c$ of the strip with the wider Au overhangs is lower than the other. This indicates that the superconducting order parameter is reduced due to the Au overhangs, and thus the Au overhangs present as normal metal at low temperature or at least should

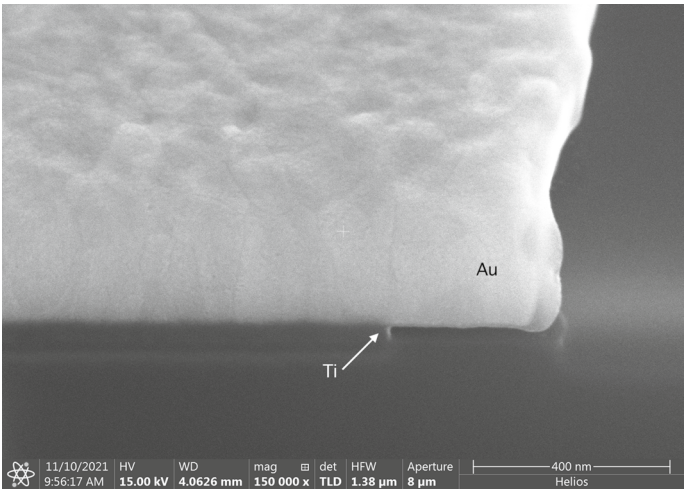


**Fig. 2** SEM image of the Au overhang structure formed by the Ti undercut. The Ti layer of this bilayer sample was etched for 12 s

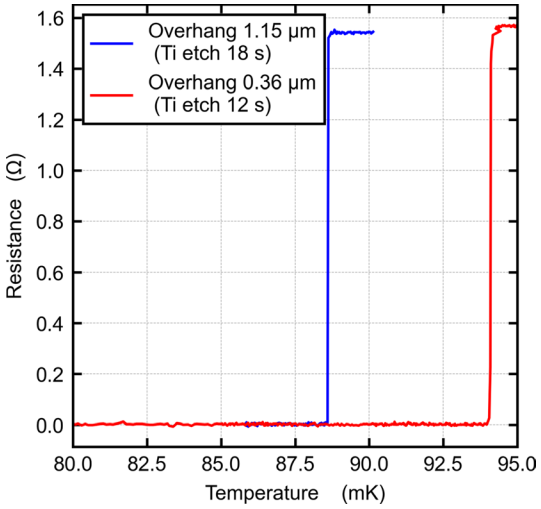


**Fig. 3** RT curves measured for the 50-µm-wide Ti/Au strips with the 0.36-µm-wide (red solid line) and 1.15-µm-wide (blue solid line) Au overhangs. The steep transition curves were observed due to very little longitudinal proximity effect induced along the long stripes [6] (color figure online)

have sufficiently lower $T_c$ than $T_{ci}$. It also means that Tc of our Ti/Au bilayer is sensitive to the width of the Au overhang so the bilayer etch process should be carefully controlled. Note that this bilayer was from stock and consists of a 41-nm-thick Ti layer to which a 270-nm-thick Au layer was added in different conditions. Therefore, $T_c$ observed in this test is not directly comparable with our main result presented in Sect. 3. Supported by these preliminary results, the Ti layer of the strips characterized in this paper was etched for 16 s, resulting a

1-μm-wide Au overhang on each side of the strip. After the sample fabrication, the actual width for each strip was inspected with an optical microscope and a SEM and determined as $W = 3.58$, 5.88, 8.28, 13.34, 18.04, 27.93 and 47.96 μm.

## 3 Measurement Results and Discussion

We measured RT curves for all the Ti/Au strips with a standard four-terminal method using a low excitation current of 1 μA. The strips were mounted on a sample holder at the cold stage of an adiabatic demagnetization refrigerator cryostat equipped with a magnetic shield at 1 K stage. The RT curves were characterized by sweeping temperature with 0.05–0.1 mK/min from the lowest temperature achieved in the cooling run to 100 mK. $T_c$ presented here for each strip was then determined as the temperature recorded at 50% of the transition.

In Fig. 4, we show the measurement result and the best fit to the data with blue dots and a black solid line, respectively. Unfortunately, we could not observe the transition for the narrowest strip with $W = 3.58$ μm because $T_c$ was too low compared with the lowest temperature of 42 mK that we could reach. Therefore, we placed this value as an upper limit on $T_c$ for this strip as marked with a blue downwards arrow from bar. This data point was not included for the fitting. The observation shows that $T_c$ starts decreasing gently from $W = 50$ μm to around $W = 20$ μm and then drops rapidly as $W$ decreases. This declining trend was well fitted with the following expression:

$$T_c/[\mathrm{mK}] = -738.4\frac{[\mu\mathrm{m}^2]}{W^2} + 91.0 \tag{1}$$

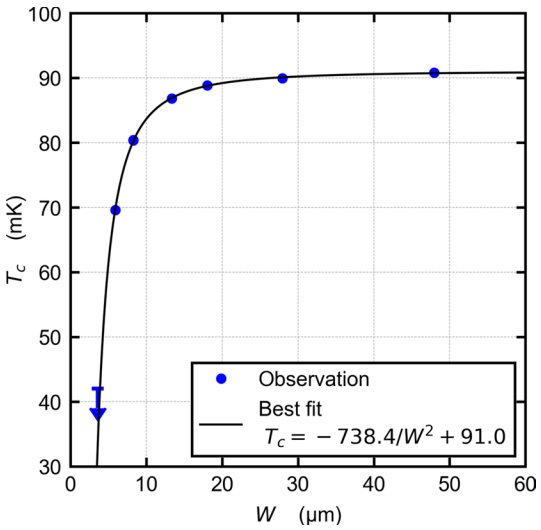


**Fig. 4** $T_c$ observed as a function of $W$ (blue dots). The data indicated with a blue downwards arrow from bar show an upper limit given by the lowest temperature we could achieve in the experiment (not included in the fit). The best-fitted curve is shown with a black solid line. The data with the upper limit were not included in the fitting (color figure online)

where $T_c(W = \infty)$ of 91 mK is consistent with $T_{ci}$ of the bilayer predicted from the ratio of the Ti and Au layer thicknesses. Based on these evident results, we concluded that the lateral inverse proximity effect exists in our Ti/Au TES due to the Au overhangs at the edge of the bilayer.

As briefly mentioned in Sect. 2, we previously studied $T_c$ affected by the longitudinal proximity effect from Nb superconducting leads [6]. We found that $\Delta T_c$ is scaled with $L$ as

$$\Delta T_{c,l}/[\mathrm{mK}] = 8418\frac{1}{L^2}. \tag{2}$$

Suppose $\Delta T_{c,l}$ and $\Delta T_{c,w}$ (defined as $\Delta T_c$ induced by the lateral inverse proximity effect) are independent from each other. $\Delta T_c$ to be observed for a rectangular-shaped Ti/Au TES can be estimated as a linear superposition of these two effect characterized as Eqs. (2) and (1):

$$\begin{aligned}\Delta T_c(L, W)/[\mathrm{mK}] =& \Delta T_{c,l}(L) + \Delta T_{c,w}(W) \\ =& 8418\frac{[\mu\mathrm{m}^2]}{L^2} - 738.4\frac{[\mu\mathrm{m}^2]}{W^2}.\end{aligned} \tag{3}$$

In Fig. 5, $\Delta T_c$ calculated by Eq. 3 is visualized in a two-dimensional parameter space consisting of $L$ and $W$. As expected, $\Delta T_c$ becomes more pronounced as $L$ and $W$ are reduced. The 3 red dots show actual measurement results for our devices. We recently produced a new batch following the fabrication details presented in Sect. 2 based on a new bilayer consists of a 42-nm-thick Ti layer to which a 300-nm-thick Au layer was added. We just started some basic functionality checks and found $\Delta T_c$

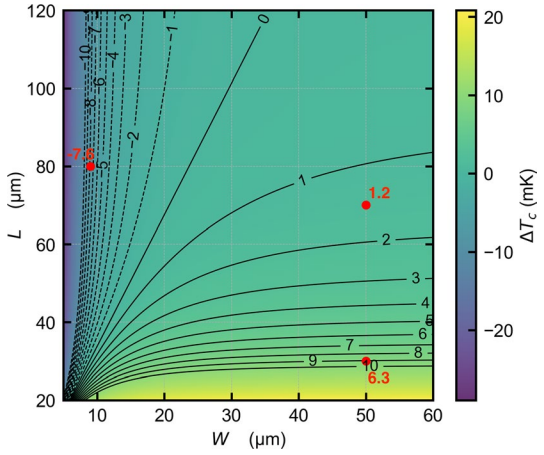


**Fig. 5** Heatmap displaying the size effect on $T_c$ for a rectangular Ti/Au TES. In a two-dimensional parameter space consisting of $L$ and $W$, $\Delta T_c(L, W) = T_c(L, W) - T_{ci}(L = \infty, W = \infty)$ calculated by Eq. (3) is visualized. To improve readability, supplementary contour lines with inline labels ($\Delta T_c$ from $-10$ to 10 mK in increments of 1 mK) are superposed on the heatmap (black dashed and solid lines). $T_c$ measurement results for 80x9, 70 × 50 and 30 × 50 μm$^2$ TESs are indicated with red dots labeled with observed $\Delta T_c$. (color figure online)

of − 7.6 mK, 1.2 mK and 6.3 mK for 80($L$) × 9($W$), 70 × 50 and 30 × 50 μm$^2$ TESs, respectively. In general, these results are in good agreement with the calculated values but there is a difference of ~ 3 mK with the shortest TES (30 × 50 μm$^2$), probably indicating that $\Delta T_{c,l}(L)$ has not been measured accurately enough. Nevertheless, this insight gives a practical overview of how much $\Delta T_c$ should be anticipated when designing TESs. It is also useful for estimating an impact of accuracy in TES patterning on $T_c$ uniformity over a TES array, although other factors such as film stress and quality of a film might be more significant.

Over the last couple of years, a TES film has no longer been considered just as an ordinary square-like film, and has become a target for optimization in its size to deliver the full potential of a TES-based instrument such as Athena/X-IFU. The optimal TES size for the main microcalorimeter array for the X-IFU instrument is under investigation with respect to many aspects: normal resistance, thermal conductance, magnetic field sensitivity [9, 10] and so on. We now have a better understanding of our Ti/Au bilayer and how much $\Delta T_c$ must be compensated in a wide range of $L$ and $W$, showing our capability of tuning $T_c$ as desired for Athena/X-IFU and other future missions.

## 4 Conclusions

We have experimentally shown that $T_c$ for our Ti/Au bilayer is suppressed as the width decreases. This is a consequence of the lateral inverse proximity effect from the normal-metal microstructures that exist as the Au overhangs at the edges of the Ti/Au bilayer. Based on the result, $T_c$ for rectangular-shaped Ti/Au TESs to be designed for future applications can be tuned more precisely, taking into account the longitudinal proximity effect from the Nb leads attached on the Ti/Au bilayer as well.

**Acknowledgements** This work is funded by the European Space Agency (ESA) under ESA CTP Contract No. 4000130346/20/NL/BW/os.

## References

1. K.D. Irwin, G.C. Hilton, *Topics in Applied Physics: Cryogenic Particle Detection* (Springer, Berlin, 2005)
2. J.E. Sadleir, S.J. Smith, S.R. Bandler, J.A. Chervenak, J.R. Clem, Phys. Rev. Lett. **104**, 047003 (2010). https://doi.org/10.1103/PhysRevLett.104.047003
3. J.E. Sadleir, S.J. Smith, K. Robinson, F.M. Finkbeiner, J.A. Chervenak, S.R. Bandler, M.E. Eckart, C.A. Kilbourne, Phys. Rev. B **84**, 184502 (2011). https://doi.org/10.1103/PhysRevB.84.184502
4. D. Barret, T.T. Lam, J.W. den Herder et al., Proc. SPIE **106991G**, 15 (2018). https://doi.org/10.1117/12.2312409
5. M. de Wit, L. Gottardi, E. Taralli, K. Nagayoshi, M.L. Ridder, H. Akamatsu, M.P. Bruijn, M. D'Andrea, J. van der Kuur, K. Ravensberg, D. Vaccaro, S. Visser, J.R. Gao, J.-W.A. den Herder, J. Appl. Phys. **128**, 224501 (2020). https://doi.org/10.1063/5.0029669
6. M.L. Ridder, K. Nagayoshi, M.P. Bruijn, L. Gottardi, E. Taralli, P. Khosropanah, H. Akamatsu, J. van der Kuur, K. Ravensberg, S. Visser, A.C.T. Nieuwenhuizen, J.R. Gao, J.W.A. den Herder, J. Low Temp. Phys. **199**, 962–967 (2020). https://doi.org/10.1007/s10909-020-02401-w

7. K. Nagayoshi, M.L. Ridder, M.P. Bruijn, L. Gottardi, E. Taralli, P. Khosropanah, H. Akamatsu, S. Visser, J.R. Gao, J. Low Temp. Phys. **199**, 943–948 (2020). https://doi.org/10.1007/s10909-019-02282-8
8. .M. Durkin, J.S. Adams, S.R. Bandler, J.A. Chervenak, S. Chaudhuri, C.S. Dawson, E.V. Denison, W.B. Doriese, S.M. Duff, F.M. Finkbeiner, C.T. FitzGerald, J.W. Fowler, J.D. Gard, G.C. Hilton, K.D. Irwin, Y.I. Joe, R.L. Kelley, C.A. Kilbourne, A.R. Miniussi, K.M. Morgan, G.C. O'Neil, C.G. Pappas, F.S. Porter, C.D. Reintsema, D.A. Rudman, K. Sakai, S.J. Smith, R.W. Stevens, D.S. Swetz, P. Szypryt, J.N. Ullom, L.R. Vale, N.A. Wakeham, J.C. Weber, B.A. Young, IEEE Trans. Appl. Supercond. **29**, 1 (2019). https://doi.org/10.1109/TASC.2019.2904472
9. D. Vaccaro, H. Akamatsu, L. Gottardi, J. van der Kuur, E. Taralli, M. de Wit, M.P. Bruijn, R. den Hartog, M. Kiviranta, A.J. van der Linden, K. Nagayoshi, K. Ravensberg, M.L. Ridder, S. Visser, B.D. Jackson, J.R. Gao, R.W.M. Hoogeveen, J.W.A. den Herder, J. Low Temp. Phys. This Special Issue (2021)
10. S. Smith, et al., J. Low Temp. Phys. This Special Issue (2021)